

# CONTENTS

<b>1</b>	<b>Introduction</b>	<b>2</b>
1.1	The Problem Statement . . . . .	2
1.2	Motivation . . . . .	2
1.3	The Scope . . . . .	3
<b>2</b>	<b>Experimental Setup</b>	<b>5</b>
2.1	Setup 1 (2-D propagation) . . . . .	5
2.2	Setup 2 (3-D propagation) . . . . .	6
<b>3</b>	<b>Spectrum Based Beamforming</b>	<b>7</b>
3.1	Conventional beamformer . . . . .	10
3.2	MVDR beamformer . . . . .	10
3.3	Comparision of MVDR and Conventional beamformers . . . . .	10
3.4	Simulation Results . . . . .	11
3.4.1	Variation of Additive Noise . . . . .	11
3.4.2	Variation of number of Sensors . . . . .	15
3.4.3	Variation of propagation Frequency . . . . .	15
3.4.4	Variation of the Sensor boundary shape . . . . .	15
<b>4</b>	<b>Deconvolution based approaches</b>	<b>17</b>
4.1	DAMAS . . . . .	17
4.2	SC-DAMAS . . . . .	19
4.3	Covariance Matrix Fitting . . . . .	20
4.4	Simulation Results . . . . .	21
4.4.1	Variation of Additive Noise . . . . .	21
4.4.2	Variation of Distance from sensor array . . . . .	27
4.4.3	Variation of Sensor array Configuration . . . . .	27
<b>5</b>	<b>Conclusion</b>	<b>29</b>

# 1 INTRODUCTION

## 1.1 THE PROBLEM STATEMENT

The problem of sound source localization starts from the basic working principle by which the human auditory system is able to locate an incoming sound in a 3-Dimensional space using only the auditory information. We usually use combination of factors in harmony to estimate the location of a sound source. The pair of sensors (ears) on either side of our head records data and we use the time difference of arrival of the signal as primary information in the locating the direction of arrival (DOA). It is the most basic method used in DOA estimation.

In this thesis, various methods that are proposed in different literature are implemented and tested for robustness. Localization of acoustic sources can be estimated given the model of the medium of propagation and the received signal at different locations, or the multichannel data. The location of the sources is solved as an inverse problem using the multichannel data. The forward model for retrieving the multichannel data is simulated using the wave propagation based on Helmholtz equations.

## 1.2 MOTIVATION

A robust algorithm for acoustic source localization can have various applications. For instance, the study can be extended for Electromagnetic waves and their applications can be in the localization of sources of brain impulses.

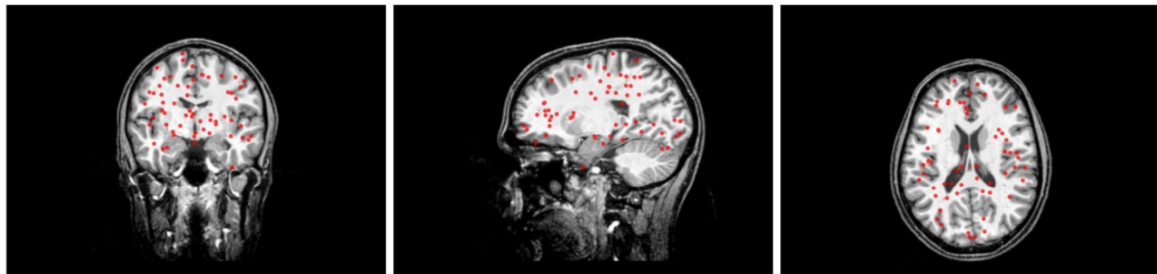


**Figure 1.1:** Position of the sources in the brain. Sources as dots, overlayed to a transparent MRI [1]

They can also be used to locate sources of abnormalities in defected lung where the defects in the bronchial airway structure act as passive sources. There is a lot of literature for modelling the lungs for the main task of localizing the sources of adversarial lung sounds. The sound transmission and the airway wall vibrations in the sub-glottal bronchial airway tree has been approximated using a 1-Dimensional branching structure proposed. Royston et al. [2],[3] studied the difference in acoustic responses for three pathological conditions in lungs, using a modified 1-Dimensional model of the bronchioles by introducing a non-self-similar structure.

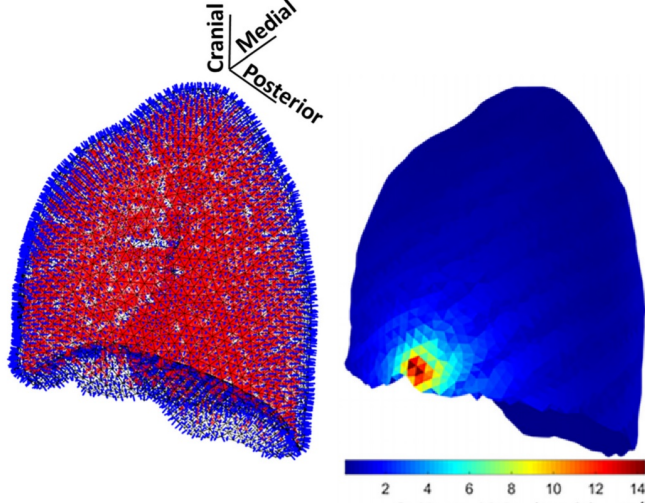


**Figure 1.2:** Modelling the Lung for defect localization [4]

In the past, The Horsfield self-similar model of the sub-glottal airway structure has been used to study the acoustic impedance throughout the tree structure [5]. According to the Horsfield model, the human bronchial airway structure contains 35 orders of segments where bifurcation takes place at every order ranging from the trachea down to the millions of alveoli. The geometric properties—diameter, length, wall thickness, cartilage fraction, degree of asymmetry in daughter branches—of the airway segments are consistent within an order.

The segments are approximated as monopole sources and a Boundary Element model is used to simulate sound propagation in the lung Parenchyma [6]. The model is simulated and the recording at the boundary elements are used to locate the passive sources in the airway tree that behave abnormally [4]. A combination of geometric, material properties and boundary condition changes were made in the airway structure to simulate the different pathological conditions [3]. A Bartlett processor is then used to estimate the location of the hypothetical monopole source inside the lung region.

### 1.3 THE SCOPE

Our main focus is to work on the algorithms for acoustic imaging. Locating acoustic sources from an array of microphones can be done using various signal processing techniques such as beamforming. Salehin et al. [7] proposed two algorithms that use the set of eigen basis function of the Helmholtz wave equation for localizing sources within a circular array of sensors. The forward scattering of sound waves is simulated based on the Helmholtz equation with their solutions employing the Green's function.

$$\nabla^2 G(x) + k^2 G(x) = -\delta(x) \text{ in } \mathbb{R}^n \quad (1.1)$$

where,  $\nabla^2$  is the Laplacian,  $k$  is the wave number,  $G(x)$  is the Green's function in  $n$  dimension,  $\delta(x)$  is the Delta dirac function.

The proposed algorithms can locate multiple sources inside the circular array of sensors and are based on the cylindrical harmonic functions. For instance, Minimum Variance Distortionless Response (MVDR) [8] beamforming can be applied on the processed sensor recordings to give an energy map corresponding to the most likely source locations in the region of survey. We also implemented deconvolution based methods that improvise on the beamforming results [9]. Another data-driven approach can be taken where a neural network is trained in two different ways; an end-to-end approach where the waveforms are directly mapped to their locations, and the other where features extracted from time domain signals are used to train the neural network model.

The simulations above are 2-dimensional with a free-field assumption. However, an acoustic behavior model imitating the lung can be incorporated into the simulation. Furthermore, the simulations can be extended to a 3-dimensional model approximating the structure and characteristics of the lung with sensor array lying on the thorax.

Various approaches for source localization are implemented in this thesis with an aim to analyze and improve the algorithms and account for their limitations.

## 2 EXPERIMENTAL SETUP

In all the simulations, the material composition of the medium are assumed to constant. Therefore, the acoustic sources will have a constant frequency and speed in the region denoted by the wave number. This is referred to as a Free Field environment where no sound reflections take place.

### 2.1 SETUP 1 (2-D PROPAGATION)

In this arrangement, the localizing of sources of sounds inside the lungs is approximated as source localization in a circular array of sensors. Here,  $Q$  microphones are placed in a circular array around the region hosting the sources [7]. It can be thought of as if the array of sensors surround the thorax in an axial plane.

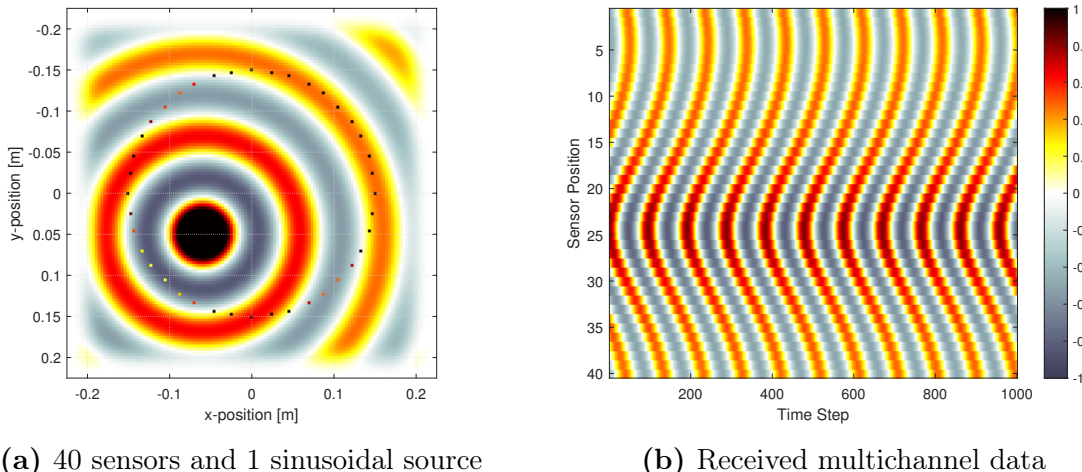


**Figure 2.1:** Setup 1

The radius of the microphone array is approximated to the radius of an average male thorax which is 15cm [7]. The canvas size is 22.5cm with a resolution of 129 x 129 grid locations. The source is sinusoidal with a frequency of 250Hz and a speed of 25m/s. The signal is recorded for 0.0419 secs with 1000 samples just enough to capture 10 peaks from the wave propagation. The data capture is started at the moment when all the microphone locations are receiving the wave propagation. These simulations of wave propagation in the time domain are performed using the k-Wave toolbox<sup>1</sup> for matlab.

The array manifold vector is computed using the solution to Helmholtz equation in  $n$ -Dimensions, given by the Green's Function. The Green's function is different depending on the dimension of the wave propagation. For this setup, since the acoustic waves

---

<sup>1</sup>k-Wave: <http://www.k-wave.org/>

propagate in a 2-Dimensional plane we use the Green's function for 2 variables given by

$$G(\mathbf{x}, \mathbf{y}, k) = \frac{i}{4} H_0^{(1)}(k|\mathbf{x} - \mathbf{y}|). \quad (2.1)$$

where, x and y corresponds to the sensor and source locations respectively.

## 2.2 SETUP 2 (3-D PROPAGATION)

This configuration of sensors and acoustic sources is considered to see the impacts of different arrangement of sensors around the sources. In this setup however, the wave propagation is not just restricted to 2-Dimensions. The forward model for acoustic sources and microphones is simulated using the solution to the Helmholtz equation in 3-Dimensions.

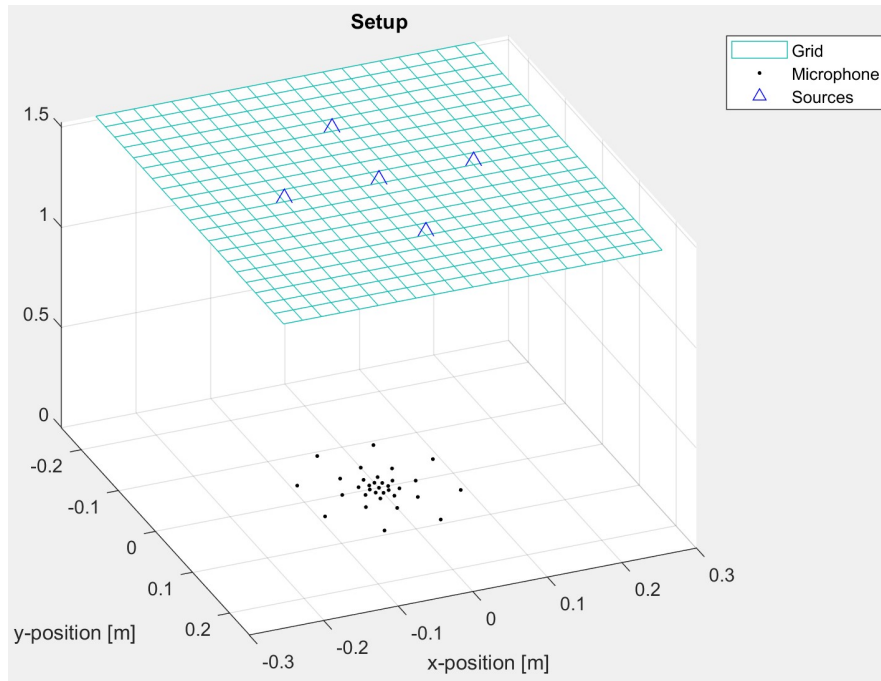


**Figure 2.2:** Configuration with 33 sensors and 5 sources

A total of 33 microphones are used in the setup. A microphone is placed at the center and the others are placed in 4 circles with 8 microphones on each circle such that the diameter of the enclosing circle is twice the diameter of the enclosed circle. The diameter of the largest circle is 19.4 cm. The acoustic sources are placed in a square grid of size 50.8 cm with a resolution of 2.54 cm. The plane of the sources is at 152 cm distance from the plane of the microphones [10].

### 3 SPECTRUM BASED BEAMFORMING

There are many approaches to address the acoustic source localization problem. Based on the classical literature reviews in this area[11] [12], these approaches are mainly divided into three categories: time delay based, beamforming based, and high resolution spectral imaging based methods. Time delay approaches compute the time difference of arrivals for various combinations of sensors that use a family of generalized cross correlation (GCC)[13] functions. Along with the information of the spatial arrangement of the sensors, the location of the sources can be estimated[11]. The beamforming method is used to steer the array of sensors in a particular dimension using special filtering to separate signals that have overlapping frequency content. When the beamforming output is maximal, the source is localized. Finally, for the spectral imaging method, the multiple signal classification algorithm (MUSIC)[14] has been widely employed.

A spectral search is more accurate than triangulation method from multichannel data [7]. Furthermore, methods using differences in arrival times require higher precision equipment than spectral based algorithms. A localization algorithm similar to Direction of Arrival (DOA) method is applied which not only aims to determine the angle but aims to estimate the source location  $\mathbf{y}$ . Array manifold vector contains info on the attenuation and the phase change as the wave propagates from source to the sensor. The array manifold matrix is computed using the Green's Function linking the source locations with the sensor locations as

$$\mathbf{A}(\mathbf{Y}) = \begin{bmatrix} \tilde{B}(\mathbf{x}_1, \mathbf{y}_1) & \dots & \tilde{B}(\mathbf{x}_1, \mathbf{y}_V) \\ \vdots & \ddots & \vdots \\ \tilde{B}(\mathbf{x}_Q, \mathbf{y}_1) & \dots & \tilde{B}(\mathbf{x}_Q, \mathbf{y}_V) \end{bmatrix} \quad (3.1)$$

where,  $B(x, y)$  is the Green's Function given by

$$B(\mathbf{x}, \mathbf{y}) = \frac{i}{4} \sum_{n=-\infty}^{\infty} H_n^{(1)}(kx) J_n(ky) e^{in\theta_x} e^{-in\phi_y} \quad (3.2)$$

where,  $H_n^{(1)}(.)$  is the Hankel function of the first kind for order n, and  $J_n(.)$  is the Bessel function for order n.

The above decomposition of Green's function consists of infinite terms and is known as the addition theorem for Hankel functions, valid only for  $|x| > |y|$ . The Bessel function for a finite argument approaches zero as the order n is increased to infinity. Hence, for a region of space bounded by a circular array of sensors of radius ( $\mathbf{R}$ ) with frequency ( $f$ ) and speed of propagation ( $c$ ) in the medium, the expansion (3.2) can be approximated for  $M$  number of eigen basis functions without a significant degradation in the simulated characteristics of wavefield [15].

$$M = \left\lceil \frac{\pi c R f}{c} \right\rceil \approx kR \quad (3.3)$$

where,  $k$  is the wave number defined by  $k = 2\pi f/c$  with  $c$  as the propagation speed,

The results in this section are simulated for the Setup 1 2.1. The sensors receive the acoustic wave propagation in the time domain at a particular frequency. The recorded time domain signals are Short-Time Fourier transformed. The data captured by the sensor for a time window at the any frequency  $f$  can defined as

$$z(k) = \sum_{v=1}^V a(y_v, k) s_v(k) + n(k) \quad (3.4)$$

where,  $z(k)$  is the  $Q \times 1$  vector of sensor recordings,  $n(k)$  is the  $Q \times 1$  vector containing the additive noise,  $s_v(k)$  is the phase and magnitude of the  $v^{th}$  source,  $a(y_v, k)$  is the  $Q \times V$  array manifold vector defining the wave propagation from  $v^{th}$  source location received at  $q^{th}$  sensor location. The above equation can be written in matrix notation as

$$\mathbf{z} = \mathbf{A}(\mathbf{Y})\mathbf{s} + \mathbf{n} \quad (3.5)$$

where,  $\mathbf{A}(\mathbf{Y}) = [a(y_1), \dots, a(y_V)]$ , and  $\mathbf{s} = [\mathbf{s}_1, \dots, \mathbf{s}_V]^T$ .

The sensors span the angles  $[0, 2\pi]$ . Let  $z(\theta)$  represent the sensor data for the sensor placed at angle  $\theta$ . The function is continuous and periodic in  $2\pi$  and at any time instant can be represented as

$$z(\theta) = \sum_{n=-M}^M \alpha_n^{(R)} e^{in\theta} \quad (3.6)$$

where,  $\alpha_n^{(R)}$  is the spacial Fourier coefficients for mode  $n$ . To solve for  $\alpha_n^{(R)}$  we can consider the above equation as an exponential Fourier expansion and by multipling both sides by  $e^{-in\theta}$  then integrating with respect to  $\theta$  we get

$$\alpha_n^{(R)} = \frac{1}{2\pi} \int_0^{2\pi} z(\theta) e^{-in\theta} d\theta \quad (3.7)$$

Using (3.4), we can also represent  $z(\theta)$  as

$$z(\theta) = \sum_{v=1}^V B((R, \theta), \mathbf{y}_v) s_v + n(\theta) \quad (3.8)$$

where,  $n(\theta)$  is the white Gaussian noise added at for a sensor at angle  $\theta$ . Using (3.2), the above equation can be written as

$$\alpha_n^{(R)} = \frac{i}{8\pi} H_n^{(1)}(kR) \sum_{v=1}^V J_n(ky_v) e^{-in\phi_v} + \tilde{n}_n \quad (3.9)$$

where,  $\tilde{n}_n$  is the noise for spacial Fourier coefficient,  $\alpha_n$ , for mode  $n$ . The above equation can be vectorized into

$$\boldsymbol{\alpha} = \mathbf{H}\mathbf{J}\mathbf{s} + \hat{\mathbf{n}} \quad (3.10)$$

where,

$$\alpha = 8\pi/i \left[ \alpha_{-M}^{(R)}, \dots, \alpha_M^{(R)} \right]^T \quad (3.11)$$

$$\mathbf{H} = \text{diag} \left[ H_{-M}^{(1)}(kR), \dots, H_M^{(1)}(kR) \right] \quad (3.12)$$

$$\mathbf{J} = \begin{bmatrix} J_{-M}(ky_1) e^{iM\phi_1} & \dots & J_{-M}(ky_V) e^{iM\phi_V} \\ \vdots & \ddots & \vdots \\ J_M(ky_1) e^{-iM\phi_1} & \dots & J_M(ky_V) e^{-iM\phi_V} \end{bmatrix} \quad (3.13)$$

The spacial Fourier coefficients are dependent on both the position of sources ( $y_v, \phi_v$ ) as well as the position of the sensors ( $R, \theta$ ). The contributions of the sensor location can be removed based on the fact that (3.9) can be simplified to (3.10). Each element of the array manifold matrix is calculated from the summation of orthogonal basis functions of 2-Dimensional wave fields (3.2). This implies that  $A(\mathbf{Y})$  can be written as a product of two matrices

$$\mathbf{A}(\mathbf{Y}) = \frac{i}{4} \mathbf{\Gamma} \mathbf{\Upsilon} \quad (3.14)$$

where,

$$\mathbf{\Gamma} = \begin{bmatrix} H_{-M}^{(1)}(kR) e^{-iM\theta_1} & \dots & H_M^{(1)}(kR) e^{iM\theta_1} \\ \vdots & \ddots & \vdots \\ H_{-M}^{(1)}(k) e^{-iM\theta_Q} & \dots & H_M^{(1)}(kR) e^{iM\theta_Q} \end{bmatrix} \quad (3.15)$$

and

$$\mathbf{\Upsilon} = \begin{bmatrix} \mathbf{J}_{-M}(ky_1) e^{iM\phi_1} & \dots & \mathbf{J}_{-M}(ky_V) e^{iM\phi_V} \\ \vdots & \ddots & \vdots \\ \mathbf{J}_M(ky_1) e^{-iM\phi_1} & \dots & \mathbf{J}_M(ky_V) e^{-iM\phi_V} \end{bmatrix} \quad (3.16)$$

Further, we transfer the sensor data to the eigen basis domain  $\tilde{\boldsymbol{\alpha}}$  by

$$\tilde{\alpha} = 4/i \Gamma^\dagger z \quad (3.17)$$

where,  $\Gamma^\dagger$  represents the Moore-Penrose pseudo-inverse of  $\Gamma$ .

An estimate of the covariance matrix is calculated in the eigen space domain. This is can be improved by increasing the number of windows ( $I$ ) used in the computation of STFT. The covariance matrix  $\mathbf{R}_{\tilde{\alpha}}$  can be estimated by using

$$\mathbf{R}_{\tilde{\alpha}} \approx \frac{1}{I} \sum_{i=1}^I \tilde{\boldsymbol{\alpha}}(i) \tilde{\boldsymbol{\alpha}}(i)^* \quad (3.18)$$

### 3.1 CONVENTIONAL BEAMFORMER

An alternative for the MVDR/Capon's beamformer is the conventional beamformer of the Bartlett beamformer. It is a natural extension of the conventional spectral analysis (spectrogram) to an array of sensors. The spectral power is given by

$$Z_{bartlett}(y, \phi) = \mathbf{c}(y, \phi)^* \mathbf{R}_{\tilde{\alpha}} \mathbf{c}(y, \phi) \quad (3.19)$$

where,

$$\mathbf{c}(y, \phi) = \begin{bmatrix} J_{-M}(ky)e^{iM\phi} \\ \vdots \\ J_M(ky)e^{-iM\phi} \end{bmatrix} \quad (3.20)$$

### 3.2 MVDR BEAMFORMER

The Minimum Variance Distortionless Response (MVDR) beamformer or the Capon's beamformer [14] was developed to account for then existing low resolution methods. This beamformer reduces the power of the reception from locations excluding the viewing region. The output power for the region denoted by the radial coordinates  $y$  and  $\phi$  is given by

$$Z_{capon}(y, \phi) = \frac{1}{\mathbf{c}(y, \phi)^* \mathbf{R}_{\tilde{\alpha}}^{-1} \mathbf{c}(y, \phi)} \quad (3.21)$$

Though the Bartlett beamformer is less complex than the Capon beamformer due to the absence of a full-rank matrix inversion, the Capon beamformer can achieve higher resolution.

### 3.3 COMPARISON OF MVDR AND CONVENTIONAL BEAMFORMERS

The MVDR beamforming spectrum and the Conventional beamforming spectrum for the source location depicted in Fig 2.1a is shown in Fig 3.1. The difference in the resolution of Fig 3.1a and Fig 3.1b is the reason we will only use the MVDR/Capon's beamformer in all future simulations in this report.

Please note that the for these results the time domain data is not used. A forward scattering model was simulated with additive noise of 20db (SNR) according to (3.5). The  $\mathbf{s}$  matrix containing the source phase and magnitude is filled with required value at the required source locations for the desired frequency. In this case,  $I$  random values following a gaussian distribution are generated for each source location to get similar values for if we perform STFT on the time domain signal. Therefore, we can increase  $I$ , the number of windows, to get an improved localization. For the following results the number of windows is fixed to 300. The frequency domain data is then used for the estimation of the covariance matrix in the eigen space domain using (3.18).

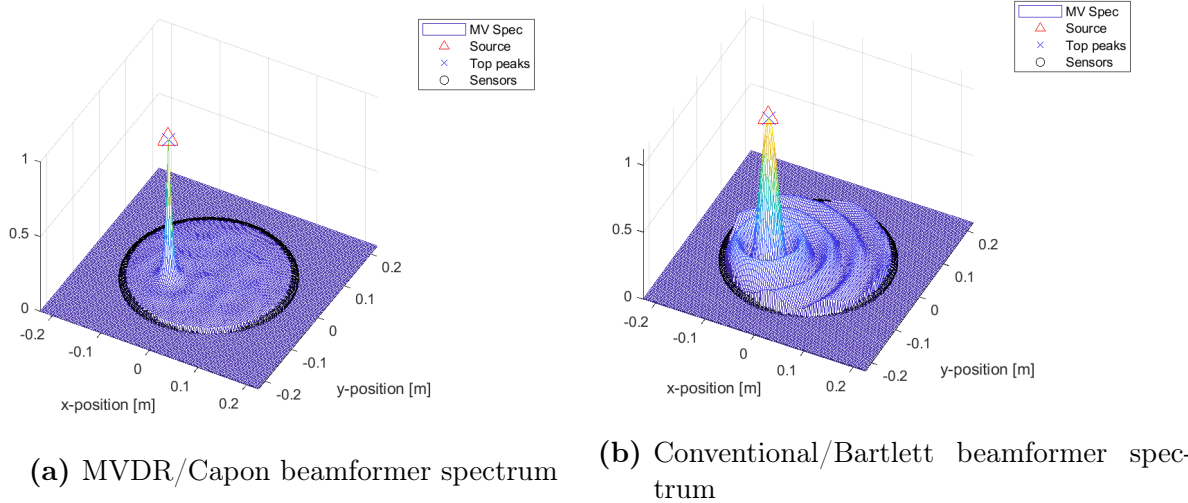


**Figure 3.1:** Beamforming spectrums with SNR: 20db

## 3.4 SIMULATION RESULTS

### 3.4.1 VARIATION OF ADDITIVE NOISE

We use the MVDR beamformer for the localization of multiple sources. We plot the estimations for varying additive noise SNR levels and try to observe any effect on the quality of predictions in Figs. 3.2 - 3.4. We see that as the noise levels are increased, there is more ambiguity in the peaks of the power spectrum. In other words, the MV spectrum resolution degrades with increase in additive noise.

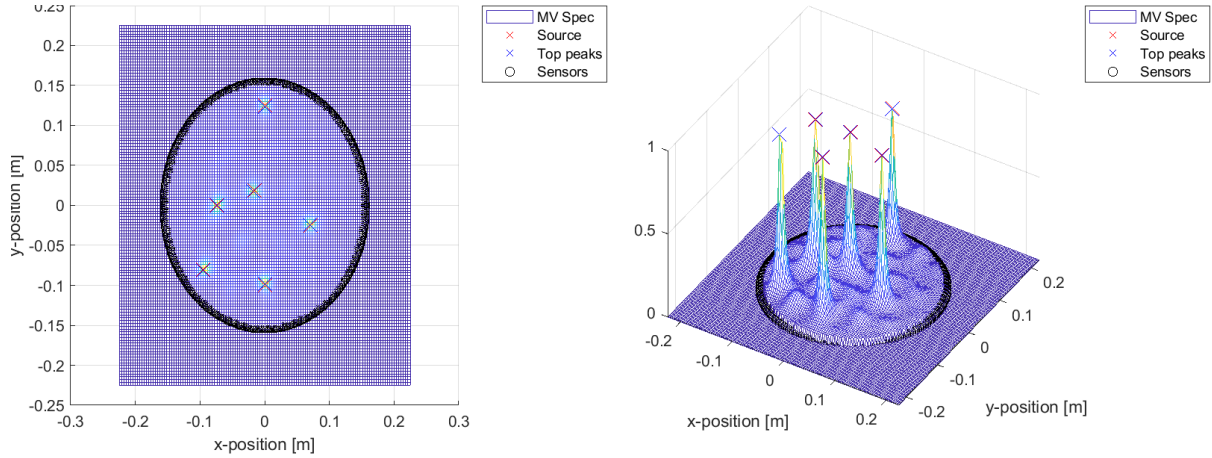


**Figure 3.2:** MV spectrum for 6 sources with 40 sensors, frequency = 250Hz and SNR: 20db

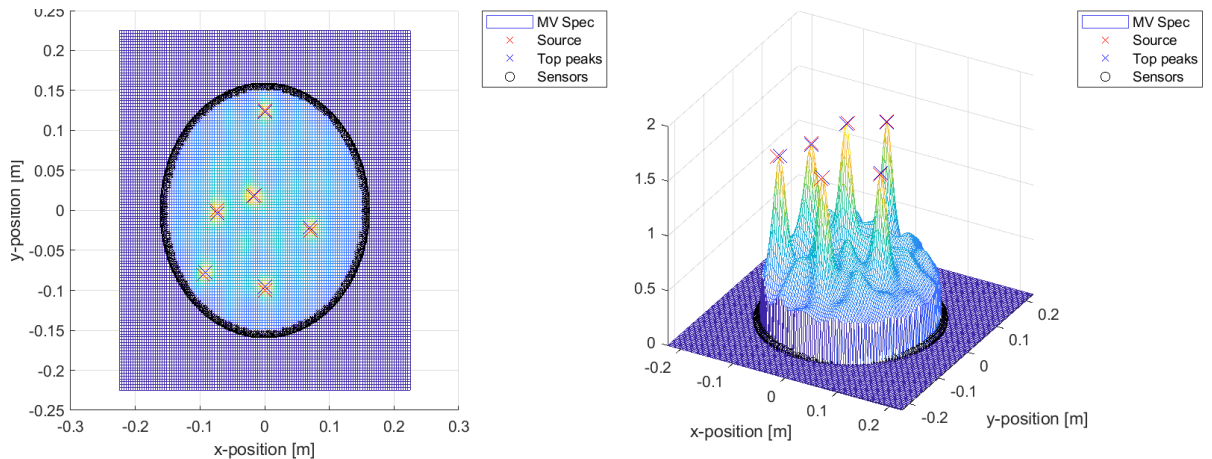


**Figure 3.3:** MV spectrum for 6 sources with 40 sensors, frequency = 250Hz and SNR: 10db

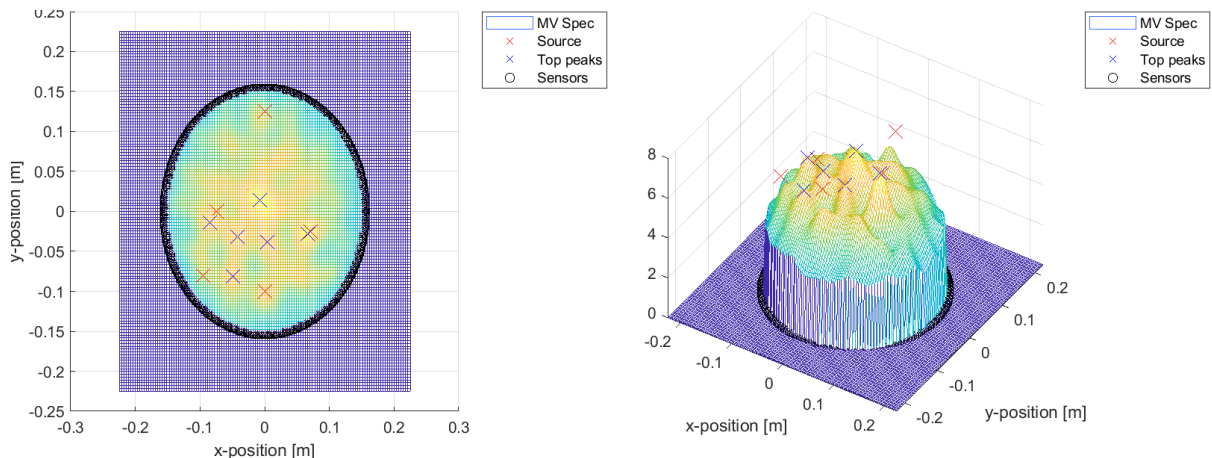


**Figure 3.4:** MV spectrum for 6 sources with 40 sensors, frequency = 250Hz and SNR: 0db

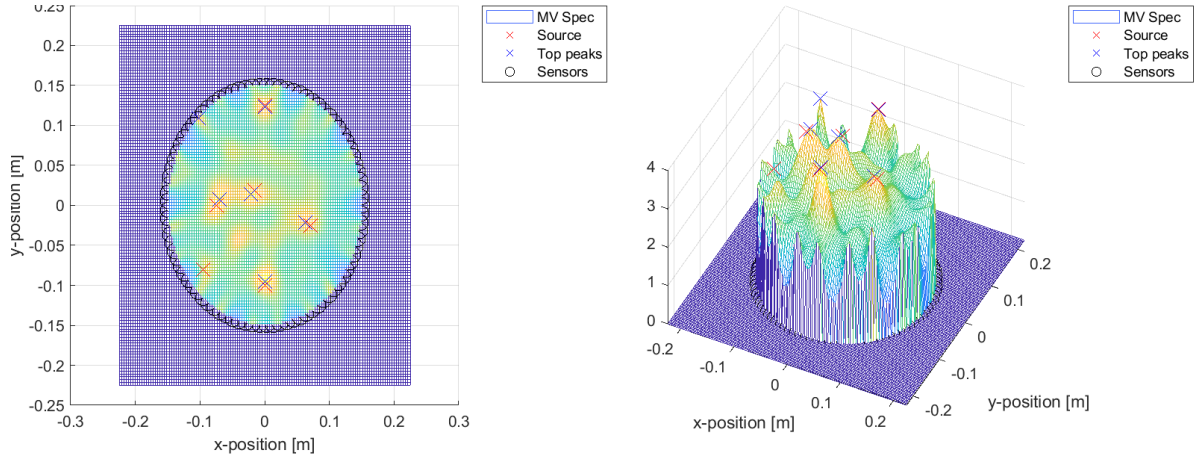


**Figure 3.5:** MV spectrum for 6 sources with 10 sensors, frequency = 250Hz and SNR: 10db

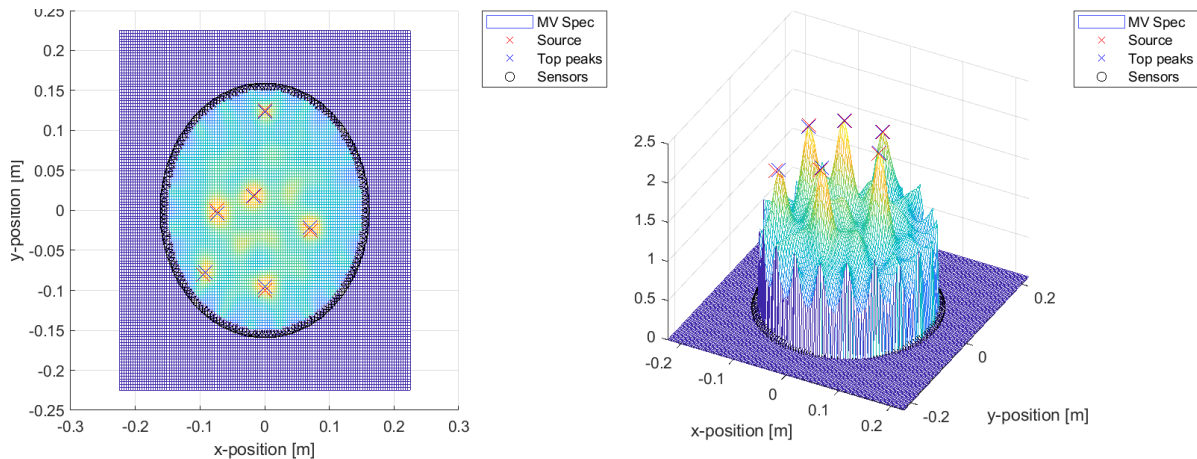


**Figure 3.6:** MV spectrum for 6 sources with 20 sensors, frequency = 250Hz and SNR: 10db

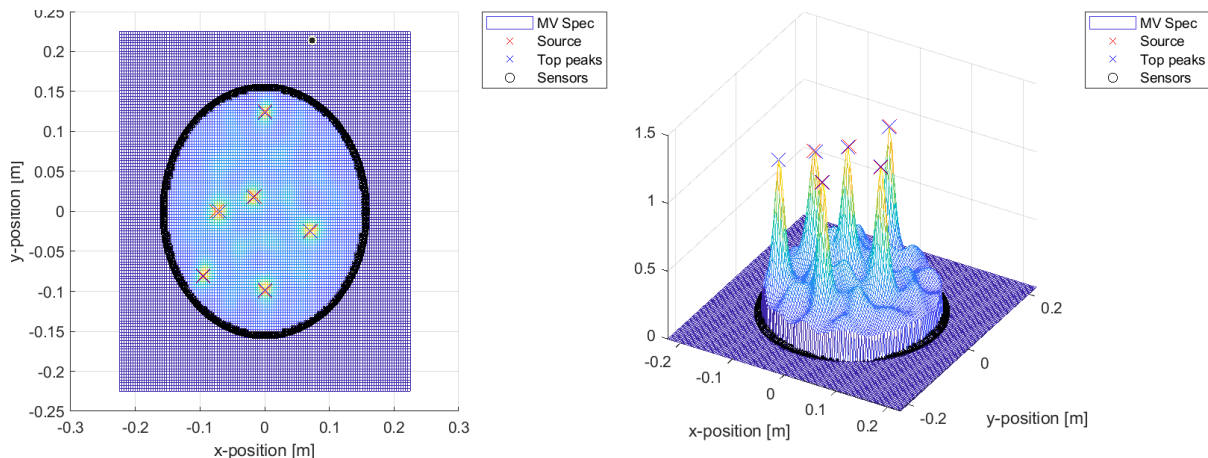


**Figure 3.7:** MV spectrum for 6 sources with 80 sensors, frequency = 250Hz and SNR: 10db

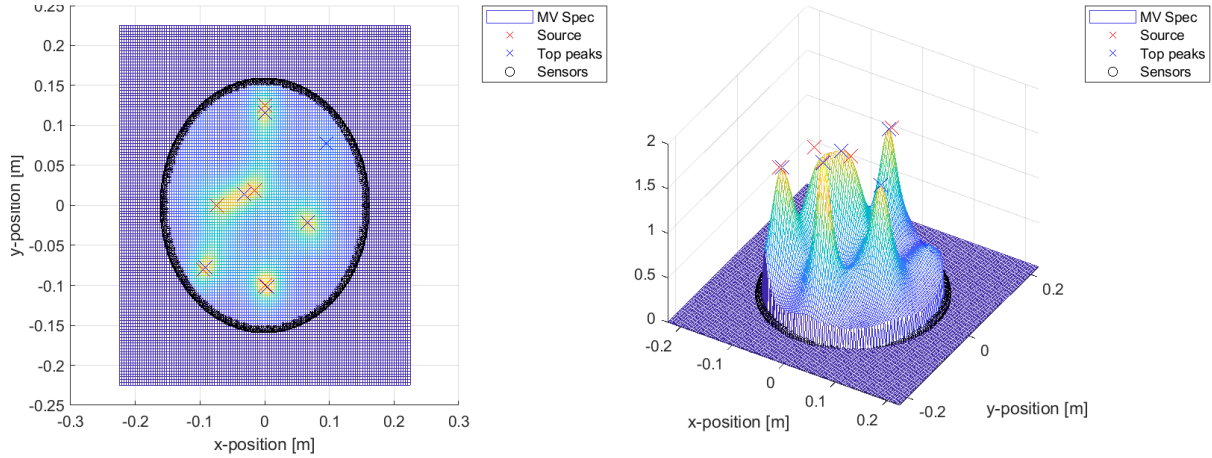


**Figure 3.8:** MV spectrum for 6 sources with 40 sensors, frequency = 150Hz and SNR: 10db

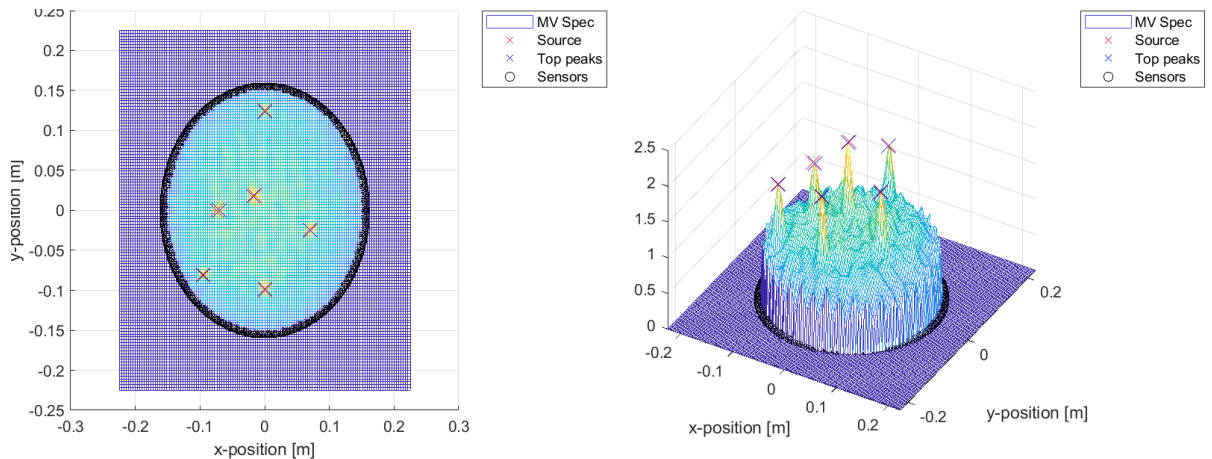


**Figure 3.9:** MV spectrum for 6 sources with 40 sensors, frequency = 500Hz and SNR: 10db

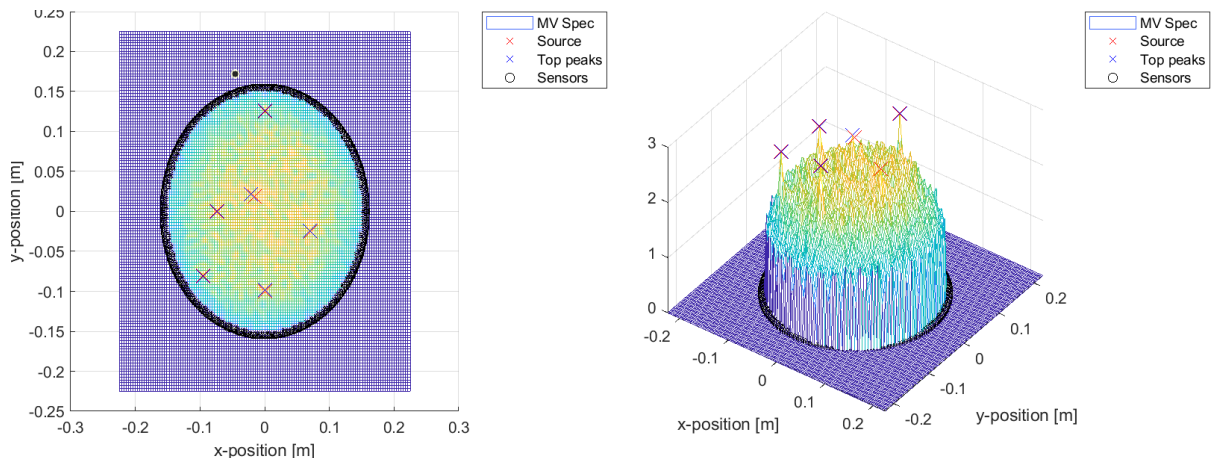


**Figure 3.10:** MV spectrum for 6 sources with 40 sensors, frequency = 1000Hz and SNR: 10db

### 3.4.2 VARIATION OF NUMBER OF SENSORS

The above results are simulated with 40 sensors. However, based on the Nyquist Criteria [7] it is observed that the resolution is also dependent on the number of sensors used to capture the acoustic data. The effect of number of sensors, for a fixed SNR of 10db, on the spectrum resolution can be seen in Figs. 3.5 - 3.7. We observe that the resolution increases with an increase in the number of sensors.

### 3.4.3 VARIATION OF PROPAGATION FREQUENCY

Furthermore, the MV power spectrum is also dependant on the frequency of the acoustic source. The wave number is a function of the desired frequency for the propagation waves in the medium. The above simulations are at a frequency of 250Hz. We can see the affect of change in the source frequency, for a fixed SNR of 10db and 40 sensor, in Figs. 3.8 - 3.10. We observe an increase in resolution of the MV spectrum with an increase in frequency of the wave propagation.

These results are coinciding with the deductions made in [7].

### 3.4.4 VARIATION OF THE SENSOR BOUNDARY SHAPE

We also changed the shape of the surrounding sensor array to observe their effects on the MV power spectrum. In the previous section, a circular sensor array is used to record the multichannel data and simulate the results. The Figs. 3.11-3.13 show the MV spectrum for different shapes of sensor array.

We observe a circular pattern in the MV spectrum when there is a change in the shape of sensor array. The shape is somehow affecting the MV spectrum by limiting the region of estimation. Any source outside this "circular-shadow" is able to get a peak in the power spectrum. However, to some extent the direction of source is correct in most cases but still not enough for source localization. It seems that the size of this "circular-shadow" is bounded by the sensor positions and transforming the ellipsoidal array 3.12 to a circular array 3.2, gives the maximum region for source localization.

In future work, the extent of influence of the array shape on the region of source location estimation using MVDR beamforming can be studied further.

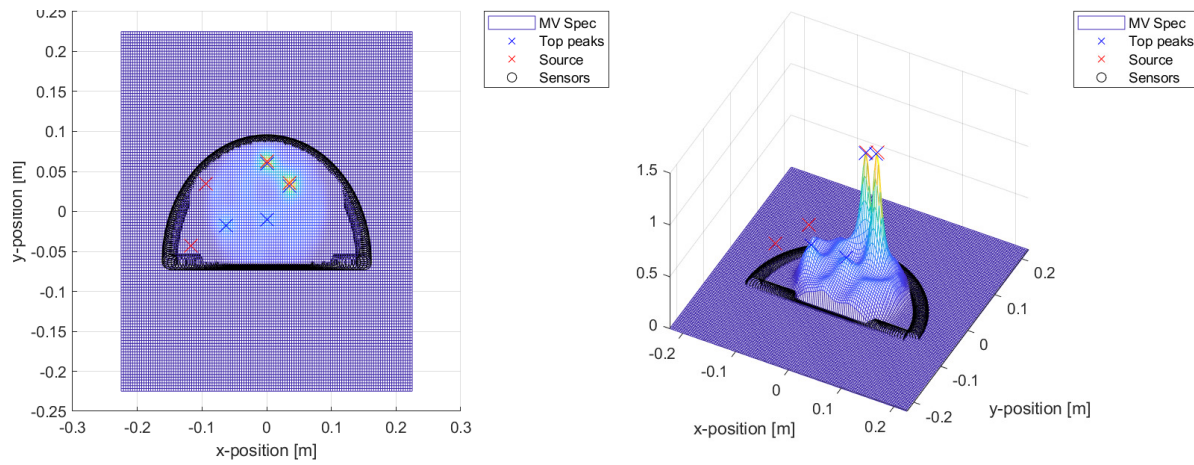


**Figure 3.11:** MV spectrum for 4 sources with semi-circular array of sensors

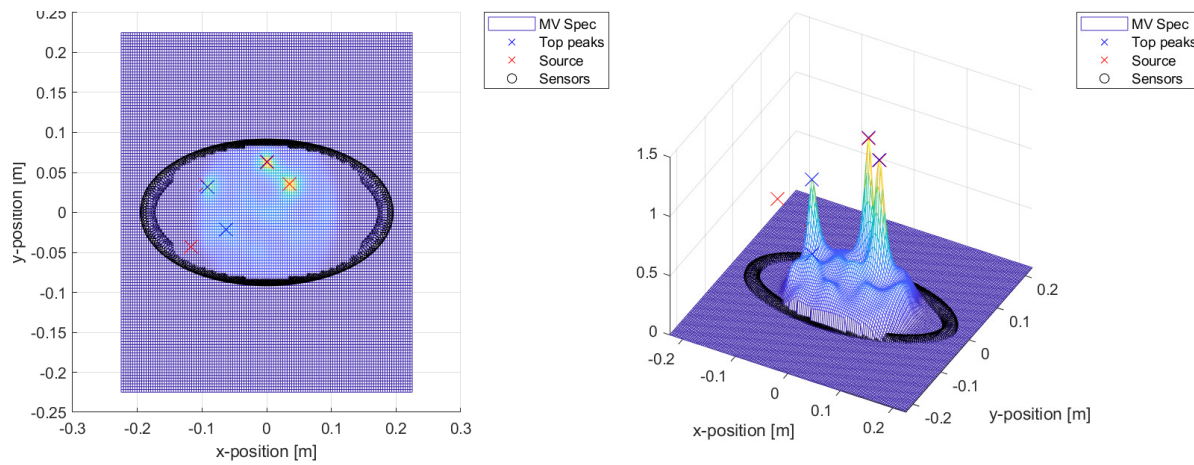


**Figure 3.12:** MV spectrum for 4 sources with ellipsoidal array of sensors

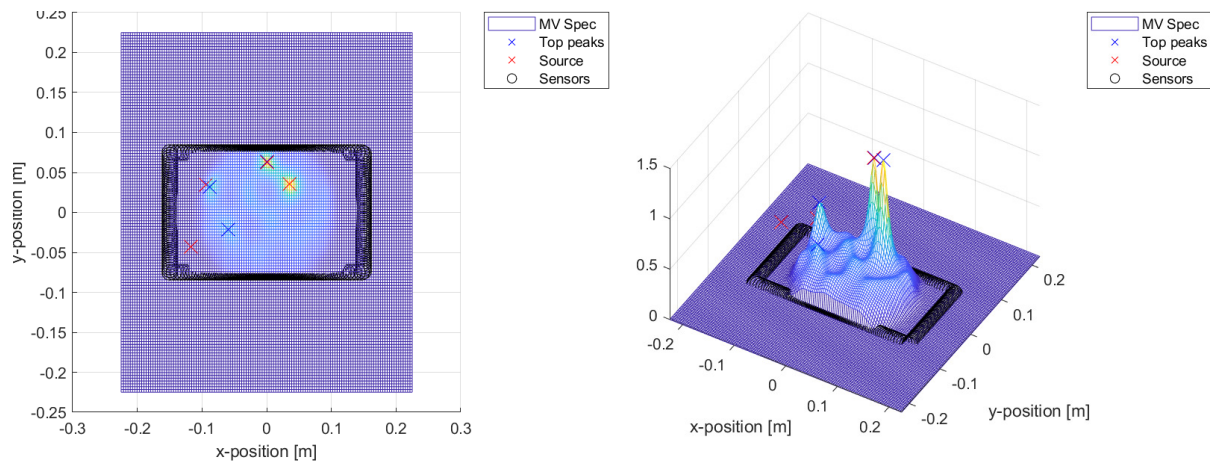


**Figure 3.13:** MV spectrum for 4 sources with rectangular array of sensors

## 4 DECONVOLUTION BASED APPROACHES

The deconvolution techniques were developed to improve the poor interpretation of the source mapping in the beamforming based methods. Although computationally effective, the acoustic source map computed by beamforming techniques exhibit a large main lobe and strong side lobes for lower frequencies [16]. This poses problems in cases with multiple close sources, where the lobes can merge and prevent source separation. Furthermore, a larger lobe can hide smaller lobes or multiple smaller lobes can merge to form a big lobe causing a false localization [16]. These drawbacks are due to what is called the Point Spread Function (PSF) of the beamformer output spectrum, which occurs when spatial array response is convolved with a single point source.

The Deconvolution Approach for the Mapping of Acoustic Sources (DAMAS) [10] iteratively deconvolves the PSF and then extracts the source distribution from the delay-and-sum (DAS) beamformer spectrum. The DAMAS is usually solved as an inverse problem using the iterative Gauss-Seidel method. The computation time can be large depending on the optimization threshold for the error.

The  $v$  sources are located at coordinates given by  $\mathbf{y}$ . The signals are received by the sensors in time domain. Then, it is divided into  $I$  windows of fixed time duration of  $L$  samples and then Discrete Fourier Transformation (or FFT) is performed on each of these windows. In this arrangement, in the presence of additive noise, the  $Q \times 1$  array output vector of an  $Q$  element microphone array can be represented as

$$\mathbf{z}_i(\omega_l) = \mathbf{A}(\mathbf{y}, \omega_l) \mathbf{s}_i(\omega_l) + \mathbf{n}_i(\omega_l), \quad i = 1, \dots, I \quad (4.1)$$

where,  $\omega_l$  is the radial frequency with  $l = 1, 2, \dots, L$ ;  $\mathbf{s}_i(\omega_l)$  is the  $v \times 1$  vector containing the source phase and magnitude at  $\omega_l$  frequency;  $\mathbf{A}(\mathbf{y}, \omega_l)$  is the  $Q \times v$  array manifold vector defining the wave propagation from  $v^{th}$  source location received at  $q^{th}$  sensor location.

The array manifold vector is computed using the solution to Helmholtz equation in n-Dimensions, given by the Green's Function. For this setup, since the wave field propagates in a 3-Dimensional space we use the Green's Function for 3 variables given by

$$G(\mathbf{x}, \mathbf{y}, k) = \frac{e^{ik|\mathbf{x}-\mathbf{y}|}}{4\pi|\mathbf{x}-\mathbf{y}|} \quad (4.2)$$

where,  $\mathbf{x}$  and  $\mathbf{y}$  corresponds to the sensor and source locations respectively.

### 4.1 DAMAS

In 4.1, the array manifold matrix  $\mathbf{A}$ , defined  $\mathbf{A}(\mathbf{x}, \omega_l) \triangleq [\mathbf{a}(\mathbf{x}_1, \omega_l), \mathbf{a}(\mathbf{x}_2, \omega_l), \dots, \mathbf{a}(\mathbf{x}_V, \omega_l)]$ , is computed using the Green's Function in 3 variables for the Setup 2 (2.2). Therefore,

the array manifold vector for the  $v^{th}$  source is given by

$$\mathbf{a}(\mathbf{x}_v, \omega_l) = \frac{1}{C(v, l)} \begin{bmatrix} \frac{1}{x_{1,v}} e^{-j k x_{1,v}} \\ \vdots \\ \frac{1}{x_{Q,v}} e^{-j k x_{Q,v}} \end{bmatrix} = \frac{\bar{\mathbf{a}}(\mathbf{x}_v, \omega_l)}{C(v, l)} \quad (4.3)$$

where,  $k$  is the wave number;  $x_{q,v} = |x_q - y_v|$ ; and  $C(v, l)$  is the constant used to normalize the columns of the array manifold matrix  $\mathbf{A}$  and is defined as  $C(v, l) = \|\bar{\mathbf{a}}(\mathbf{x}_k, \omega_l)\|_2$

The spectral covariance matrix  $\mathbf{R}$  for a given radial frequency  $\omega_l$  is estimated from the acquired sensor data  $\mathbf{z}_i$  as

$$\hat{\mathbf{R}}(\omega_l) = \frac{1}{I} \sum_{i=1}^I \mathbf{z}_i(\omega_l) \mathbf{z}_i^H(\omega_l) \quad (4.4)$$

The estimation of the covariance matrix can be improved by increasing the number of windows  $I$ . The delay-and-sum (DAS) beamformer output power spectrum for a location  $\mathbf{x}'$  is given by

$$Z_{DAS}(\mathbf{x}', \omega_l) = \frac{1}{Q^2} \tilde{\mathbf{a}}^H(\mathbf{x}', \omega_l) \hat{\mathbf{R}}(\omega_l) \tilde{\mathbf{a}}(\mathbf{x}', \omega_l) \quad (4.5)$$

where,

$$\tilde{\mathbf{a}}(\mathbf{x}_v, \omega_l) = C(v, l) \begin{bmatrix} x_{1,v} e^{-j k x_{1,v}} \\ \vdots \\ x_{Q,v} e^{-j k x_{Q,v}} \end{bmatrix} \quad (4.6)$$

We substitute (4.1) and (4.4) in (4.5) and approximate the further approximate by neglecting the cross terms provided  $I >> 1$  and neglecting the noise terms to obtain

$$Z_{DAS}(\mathbf{x}', \omega_l) = \sum_{v=1}^V \tilde{A}_v(\mathbf{x}') \tilde{x}(\mathbf{x}_v) \quad (4.7)$$

where,

$$\tilde{x}(\mathbf{x}_v) \triangleq (1/I) \sum_{i=1}^I |s_{i,v}|^2 \quad (4.8)$$

and

$$\tilde{A}_v(\mathbf{x}') = \frac{1}{Q^2} |\tilde{\mathbf{a}}^H(\mathbf{x}') \mathbf{a}(\mathbf{x}_v)|^2, \quad v = 1, \dots, V \quad (4.9)$$

In these equations (4.5) - (4.9), the number of sources  $V$  is unknown and is generally replaced by size of the complete gridspace which is represented by  $N$ . It represents the number of grid locations to search for and therefore comprises of all possible region where the source can be present. The DAS power spectrum (4.5) is stacked to be in vectorized form represented by  $\tilde{\mathbf{Z}}$  as

$$\begin{bmatrix} \tilde{Z}(\mathbf{x}_1) \\ \tilde{Z}(\mathbf{x}_2) \\ \vdots \\ \tilde{Z}(\mathbf{x}_N) \end{bmatrix} = \begin{bmatrix} \tilde{A}_1(\mathbf{x}_1) & \tilde{A}_2(\mathbf{x}_1) & \cdots & \tilde{A}_N(\mathbf{x}_1) \\ \tilde{A}_1(\mathbf{x}_2) & \tilde{A}_2(\mathbf{x}_2) & \cdots & \tilde{A}_N(\mathbf{x}_2) \\ \vdots & \vdots & \ddots & \vdots \\ \tilde{A}_1(\mathbf{x}_N) & \tilde{A}_2(\mathbf{x}_N) & \cdots & \tilde{A}_N(\mathbf{x}_N) \end{bmatrix} \begin{bmatrix} \tilde{x}(\mathbf{x}_1) \\ \tilde{x}(\mathbf{x}_2) \\ \vdots \\ \tilde{x}(\mathbf{x}_N) \end{bmatrix} \quad (4.10)$$

or  $\tilde{\mathbf{Z}} = \tilde{\mathbf{A}}\tilde{\mathbf{X}}$ . Each term after matrix multiplication can be represented as

$$\tilde{Z}_n = \tilde{A}_{n,1}\tilde{x}_1 + \tilde{A}_{n,2}\tilde{x}_2 + \cdots + \tilde{A}_{n,N}\tilde{x}_N \quad (4.11)$$

To estimate the  $\tilde{\mathbf{X}}$  we solve this inverse problem using the Gauss-Seidel method. Note that  $\tilde{A}_{n,n} = 1$  is always true for  $\tilde{\mathbf{A}}$ . The solution for  $\tilde{\mathbf{X}}$  is given by

$$\tilde{x}_n^{(iter)} = \max \left( 0, \tilde{y}_n - \left[ \sum_{j=1}^{n-1} \tilde{A}_{nj} \tilde{x}_j^{(iter)} + \sum_{j=n+1}^N \tilde{A}_{nj} \tilde{x}_j^{(iter-1)} \right] \right) \quad (4.12)$$

The constraint of  $\tilde{x}_n$  being positive is justified by the fact that it represents the source power. The iterations can be restrained by setting a threshold to the error desired from the solution.

## 4.2 SC-DAMAS

In its most basic form, the sparse modelling can be stated as

$$\text{minimize } \|\tilde{\mathbf{X}}\|_0 \text{ subject to } \tilde{\mathbf{Z}} = \tilde{\mathbf{A}}\tilde{\mathbf{X}} \quad (4.13)$$

with  $\tilde{\mathbf{X}}$  as the unknown, it is a combinatorial problem which becomes increasingly complex as the size of  $\tilde{\mathbf{X}}$  increases. To improve the complexity, a sparsity prior can be introduced that reduces the domain space for the computation of the inverse solution [9]. If the solution is sufficiently sparse, the  $l_0$  norm can be replaced to  $l_1$  norm to make the problem convex [17]. Noting that we replaced V with N in the (4.10) and  $N \gg V$  implies that the presence of a source in the solution  $\tilde{\mathbf{X}}$  is very sparse. The  $\tilde{\mathbf{A}}$  matrix contain all the search points but only a small portion of them are supposed to hold strong sources. Therefore, an altered version of LASSO [18] can be used to structure the optimization problem as

$$\begin{aligned} & \text{minimize} && \|\tilde{\mathbf{Z}} - \tilde{\mathbf{A}}\tilde{\mathbf{X}}\|_2^2 \\ & \text{subject to} && \|\tilde{\mathbf{X}}\|_1 \leq \lambda, \quad \tilde{x}_n \geq 0, \quad n = 1, \dots, N \end{aligned} \quad (4.14)$$

where, the user parameter  $\lambda$  is a hyperparameter and can be estimated from the covariance matrix  $\tilde{\mathbf{R}}$ . The covariance matrix can be written as

$$\mathbf{R} = E \{ \mathbf{z}_i \mathbf{z}_i^H \} = \mathbf{A} \mathbf{D} \mathbf{A}^H + \sigma^2 \mathbf{I} \quad (4.15)$$

where,  $\mathbf{D} = E \{ \mathbf{s}_i \mathbf{s}_i^H \}$  represents the diagonal matrix for uncorrelated sources,

$$\mathbf{D} = \begin{bmatrix} d_1 & 0 & \cdots & 0 \\ 0 & d_2 & \cdots & 0 \\ \vdots & \vdots & \ddots & \vdots \\ 0 & 0 & \cdots & d_V \end{bmatrix} \quad (4.16)$$

where,  $d_v, v = 1, \dots, V$  is the power for the  $v^{th}$  source. The eigenvalue decomposition of  $\mathbf{ADA}^H$  can be written as  $\mathbf{ADA}^H = \mathbf{U}\Lambda\mathbf{U}^H$ , where,  $\mathbf{U}$  represents the eigenvectors and  $\Lambda$  denote the corresponding eigenvalues given by  $\lambda_1 \geq \lambda_2 \geq \dots \geq \lambda_V \geq 0$ . The  $\Lambda$  is a  $Q \times Q$  matrix where  $Q > V$ . Then the covariance matrix  $\mathbf{R}$  can be written as

$$\mathbf{R} = \mathbf{U}(\Lambda + \sigma^2 \mathbf{I}) \mathbf{U}^H \triangleq \mathbf{U}\Gamma\mathbf{U}^H \quad (4.17)$$

where the diagonal elements, the eigenvalues, of the diagonal matrix  $\Gamma$  are  $\gamma_1 \geq \gamma_2 \geq \dots \geq \gamma_V \geq \sigma^2$ . Also,

$$\text{Tr}(\Lambda) = \text{Tr}(\mathbf{U}\Lambda\mathbf{U}^H) = \text{Tr}(\mathbf{ADA}^H) = \text{Tr}(\mathbf{DA}^H\mathbf{A}) = \text{Tr}(\mathbf{D}) = \sum_{k=1}^K d_k \quad (4.18)$$

which denotes the total power of the sources.

Notice, however, we only have an estimate for the covariance matrix  $\hat{\mathbf{R}}$  given by (4.4). Therefore, let  $\hat{\Gamma}$  denote the eigenvalues matrix corresponding to  $\hat{\mathbf{R}}$  and then the hyperparameter  $\lambda$  in the (4.13) can be calculated as

$$\lambda = \text{Tr}(\hat{\Gamma} - \hat{\gamma}_M \mathbf{I}) \quad (4.19)$$

where  $\hat{\gamma}_M$  is the smallest eigenvalue from  $\hat{\Gamma}$ . This approach of optimizing (4.13) using an upper constraint on the solution in (4.19) is referred to as the Sparsity Constrained DAMAS (SC-DAMAS) [9]. The optimization of (4.13) is computed using the Self-Dual Minimization (SeDuMi) [19] toolbox available on the CVX MATLAB toolbox<sup>2</sup>

The DAMAS algorithm can be further sped up by replacing the set of the gridspace  $N$  in (4.10) by a smaller set of  $N_0$  which forms a much smaller subset of  $N$ . In other words, if we have a prior on the possible locations of the source which can reduce the survey region, this can significantly speed up the computation time by reducing the matrix size for optimization as in

$$\begin{bmatrix} \tilde{Z}(\mathbf{x}_1) \\ \tilde{Z}(\mathbf{x}_2) \\ \vdots \\ \tilde{Z}(\mathbf{x}_{N_0}) \end{bmatrix} = \begin{bmatrix} \tilde{A}_1(\mathbf{x}_1) & \tilde{A}_2(\mathbf{x}_1) & \cdots & \tilde{A}_N(\mathbf{x}_1) \\ \tilde{A}_1(\mathbf{x}_2) & \tilde{A}_2(\mathbf{x}_2) & \cdots & \tilde{A}_N(\mathbf{x}_2) \\ \vdots & \vdots & \ddots & \vdots \\ \tilde{A}_1(\mathbf{x}_{N_0}) & \tilde{A}_2(\mathbf{x}_{N_0}) & \cdots & \tilde{A}_N(\mathbf{x}_{N_0}) \end{bmatrix} \begin{bmatrix} \tilde{x}(\mathbf{x}_1) \\ \tilde{x}(\mathbf{x}_2) \\ \vdots \\ \tilde{x}(\mathbf{x}_{N_0}) \end{bmatrix} \quad (4.20)$$

where,  $N_0 \ll N$ . This can be extended to the SC-DAMAS as well in the optimization in equation (4.13).

### 4.3 COVARIANCE MATRIX FITTING

This method is **not** specifically a deconvolution based approach. Rather, here the estimated covariance matrix is directly used for formulating a convex optimization from

---

<sup>2</sup>CVX: Matlab Software for Disciplined Convex Programming. URL: <http://cvxr.com/cvx/>

the eq (4.15). The optimization problem is

$$\begin{aligned} & \text{minimize}_{[d_n]_{n=1}^N, \sigma^2} \left\| \hat{\mathbf{R}} - \mathbf{A} \mathbf{D} \mathbf{A}^H - \sigma^2 \mathbf{I} \right\|_F^2 \\ & \text{subject to } d_n \geq 0, \quad n = 1, \dots, N, \quad \sum_{n=1}^N d_n \leq \lambda, \quad \sigma^2 \geq 0 \end{aligned} \quad (4.21)$$

a quadratic convex optimization problem, where,  $\lambda$  is defined in eq (4.19),  $\mathbf{A}$  is the array manifold vector defined in eq (4.3),  $\sigma^2$  is the added noise, and the  $\mathbf{D}$  is the diagonal matrix defined by (4.16). It is  $\sigma$  along with  $\mathbf{D}$  that are adjusted to minimization of the error in (4.21).

To solve using the CMF method, we used the CVX toolbox to optimize the convex problem 4.21 with just the diagonal matrix  $\mathbf{D}$  as the variable and fixing  $\sigma$ . The adjustment of  $\sigma$  was varied separately and the value which gave minimum error in (4.21) was chosen for  $\sigma$ . In most cases the error came out to be minimum for  $\sigma = 0$ , unless the SNR was extremely low.

## 4.4 SIMULATION RESULTS

The simulations shown are performed for the Setup 2 (2.2) with  $Q = 33$  sensors, number of windows used is 10000, speed of propagation is 40m/s, and the frequency of propagation is 15kHz. The gridspace containing the sources is at a perpendicular distance of 1.52m (depth) from the plane of the sensors as explained in Section 2.2.

### 4.4.1 VARIATION OF ADDITIVE NOISE

The DAMAS, SC-DAMAS, CMF, DAS along with the MVDR (3-Dimensional setup) source localization with varying SNR levels are shown in the Figs. 4.1 - 4.3.

Please note that for CMF results, the optimization is computed using the CVX toolbox with  $\sigma$  ranging from 0 to 10 in steps of 0.5. The plot titles contain the value for  $\sigma$  for which the error in optimization was minimum.

Notice, the peaks in the SC-DAMAS mapping are sharp with low ambiguity in contrast to the DAMAS method. This is due to the constraint put on the source mapping by  $\lambda$ . However, the CMF performs better than both DAMAS and SC-DAMAS methods with increase in noise [9].

On one hand, the peak separation in the mapping from the DAS methods does not seem to improve with reduction in noise. While the MVDR method shows sharp peaks with decreasing ambiguity in mapping with decrease in noise. This shows that MVDR can achieve better resolution with improvement in the noise.

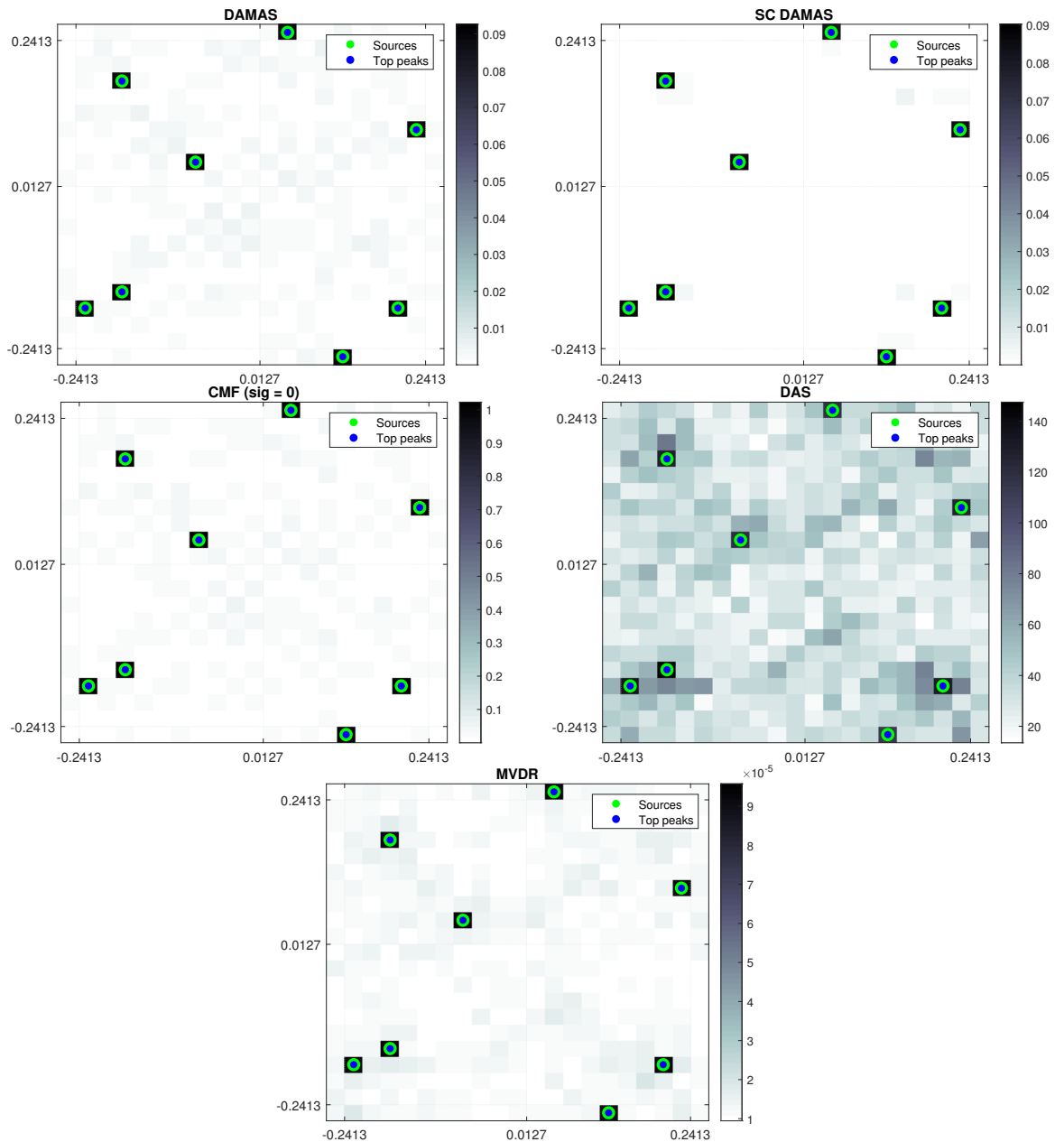


**Figure 4.1:** Acoustic Mapping with depth of 1.52m and SNR: 20db

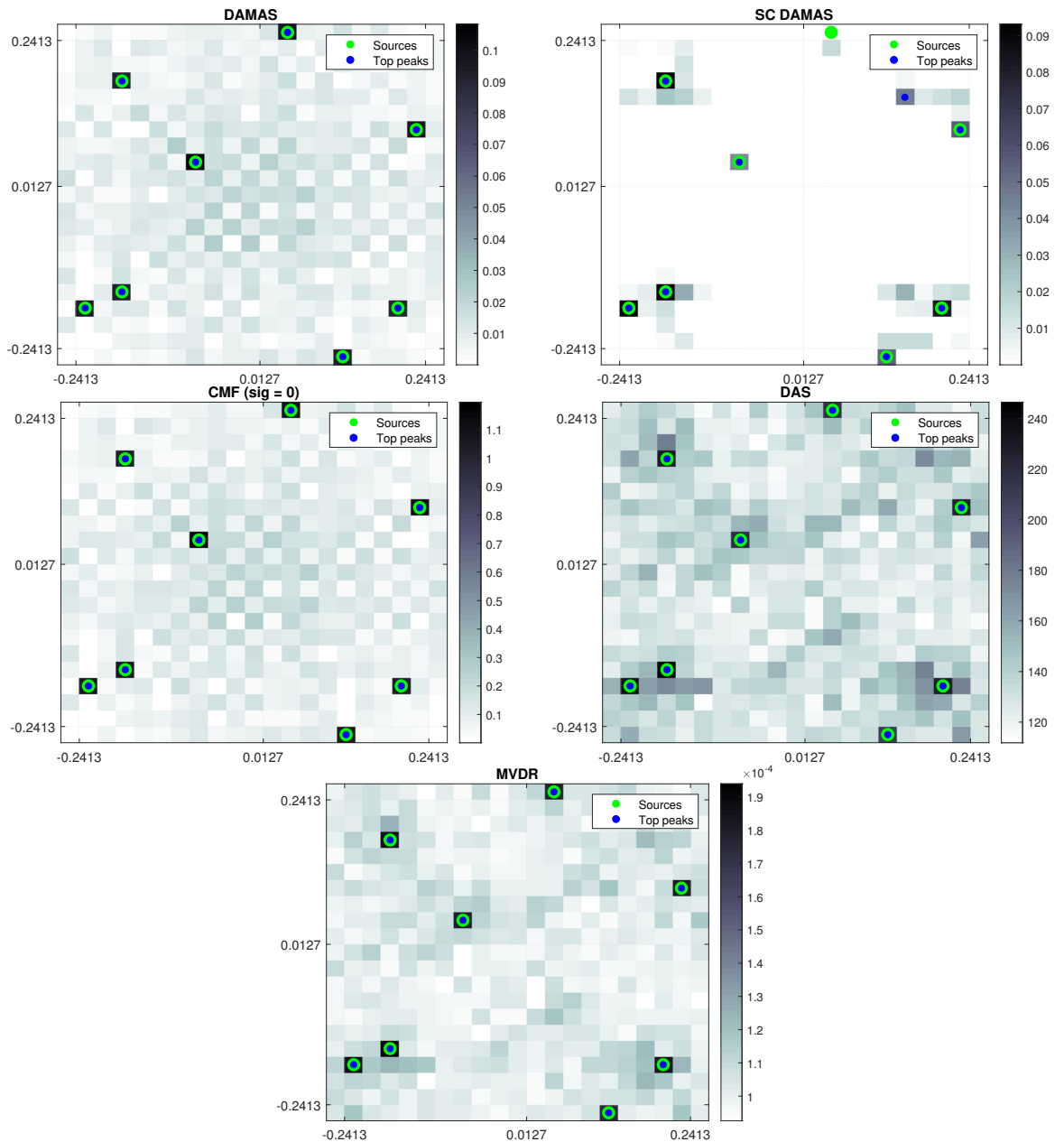


**Figure 4.2:** Acoustic Mapping with depth of 1.52m and SNR: 10db

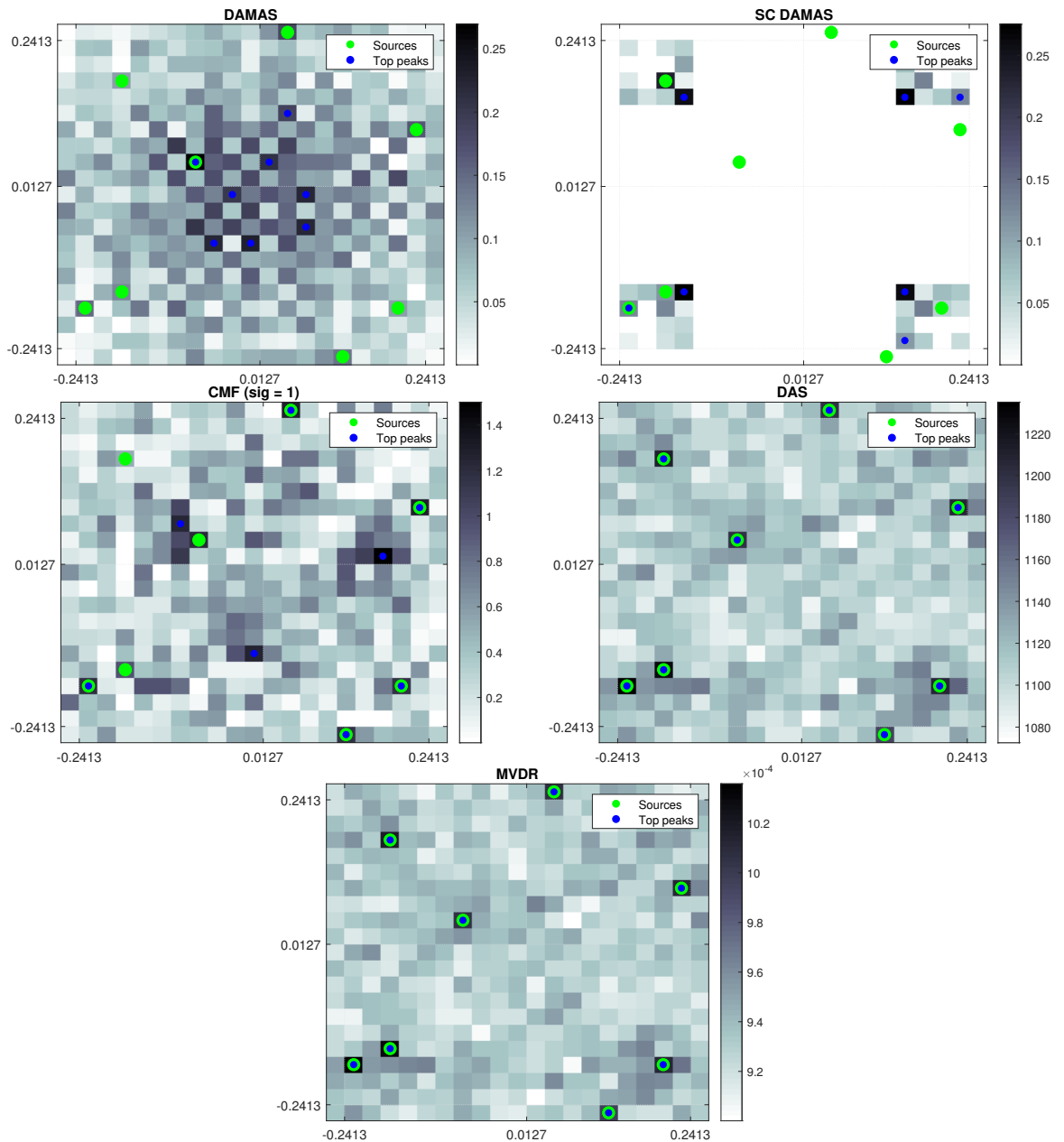


**Figure 4.3:** Acoustic Mapping with depth of 1.52m and SNR: 0db

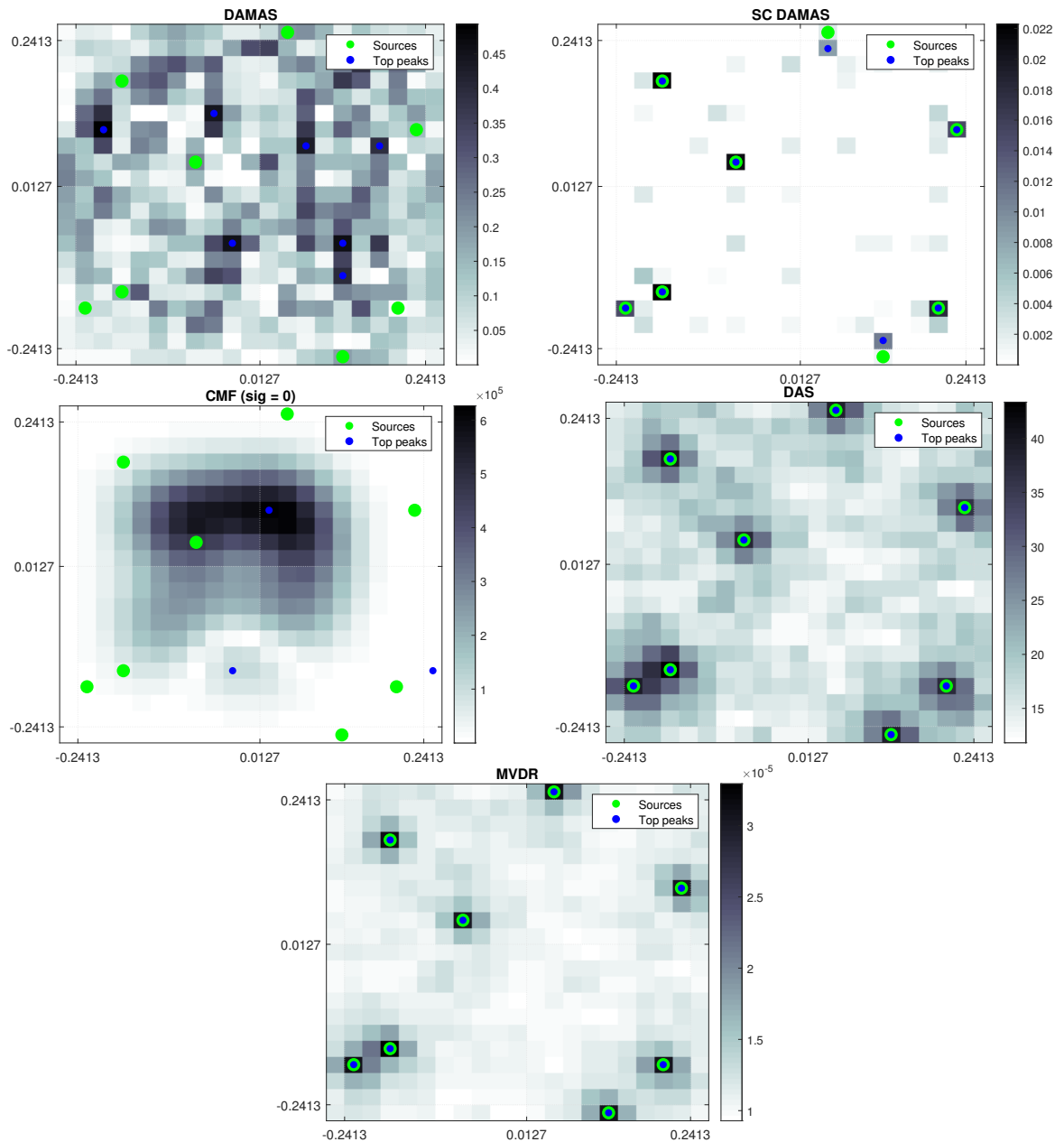


**Figure 4.4:** Acoustic Mapping with depth of 3.04m and SNR: 20db

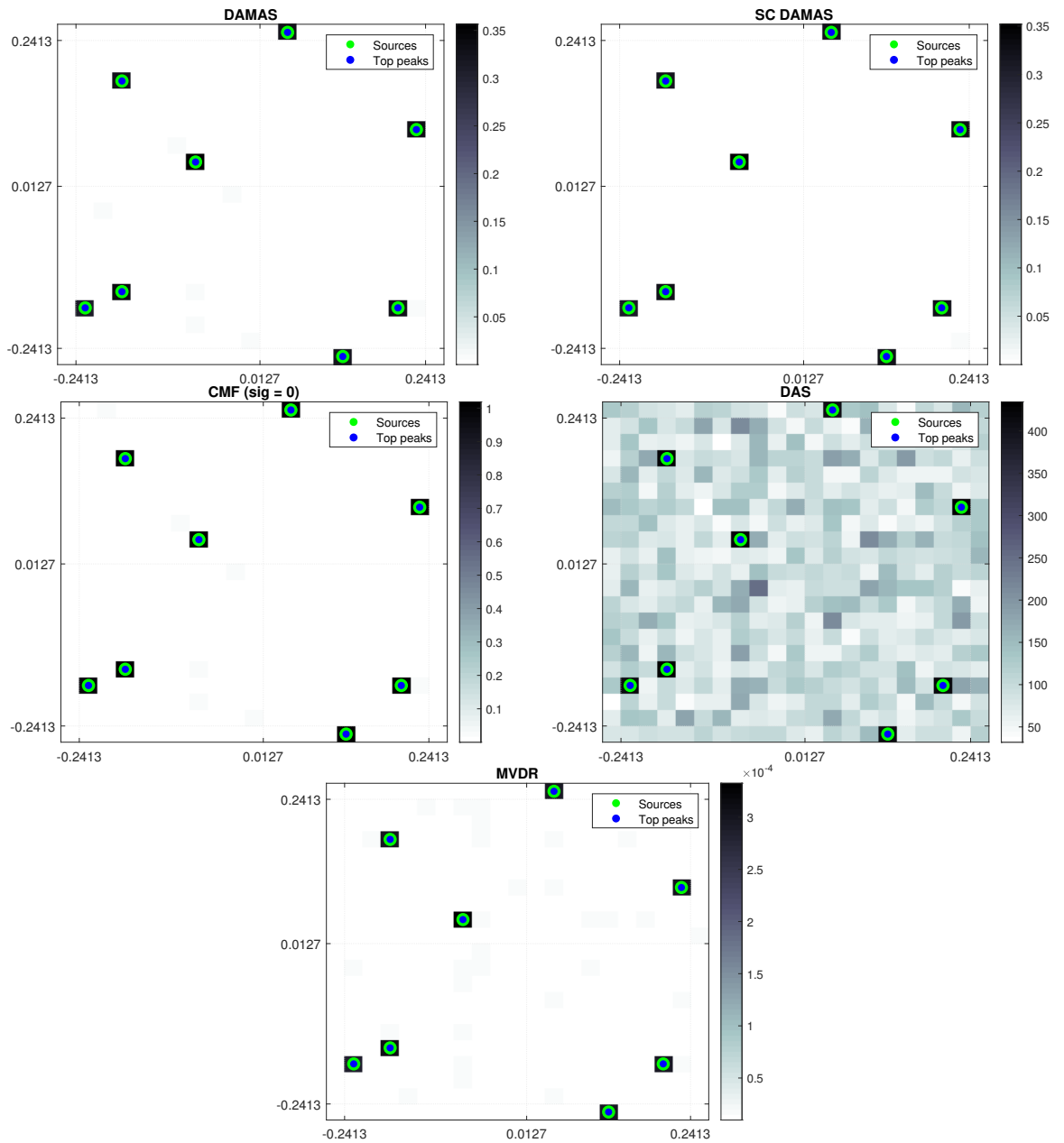


**Figure 4.5:** Acoustic Mapping with depth of 0.76m and SNR: 20db

#### 4.4.2 VARIATION OF DISTANCE FROM SENSOR ARRAY

The Fig 4.4,4.5 depict the variation in the imaging when the sources are at a distance of 3.04m and 0.76m respectively. We see a drastic degradation in the imaging when the distance is increased to 3.04m for DAMAS, SC-DAMAS and CMF methods. However, the DAS and MVDR performed with a lower resolution but accurate localization. Further we observe, reducing the source distance from the sensors increases the resolution of all the methods in Fig 4.5.

#### 4.4.3 VARIATION OF SENSOR ARRAY CONFIGURATION

In this modification, the sensor array is transitioned from its arrangement in Setup 2 (2.2) to the sensor arrangement in Setup 1 (2.1). In other words, the sensors are now placed around in a circular array around and in the same plane as the gridspace hosting the sources Fig. 4.6. This is the same configuration as in Setup 1, except for the fact that the wave propagation will still occur in 3-Dimensions. We return to this configuration in order to focus on the performance of these algorithms for a setup where the sources are enclosed by an array of sensors.

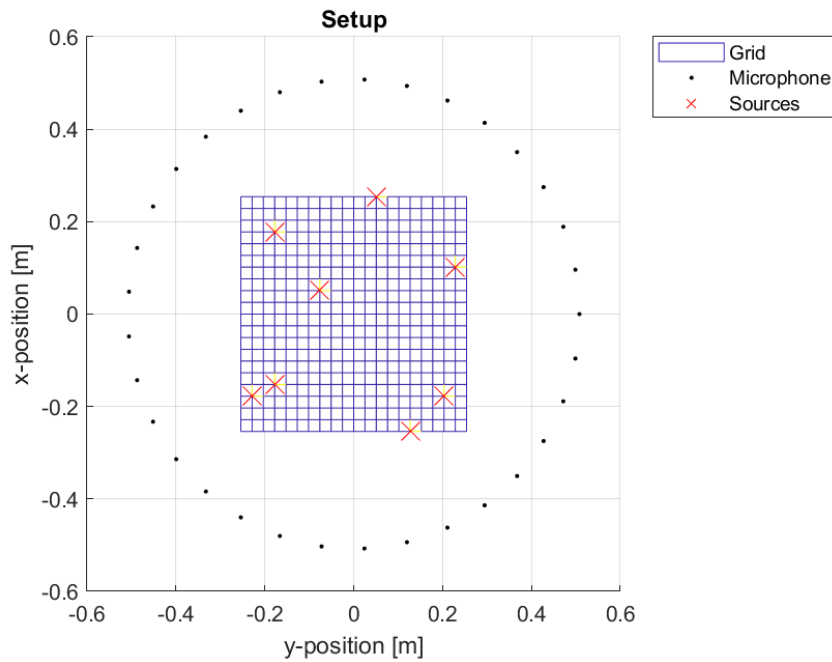


**Figure 4.6:** The changed arrangement in Setup 2

In this simulation, the same number of 33 sensors are used to form a circular array with a radius equivalent to the side of the gridspace (i.e. 50.4cm). We could not implement DAMAS method because the Gauss-Seidel optimization turned out to be divergent for this setup. The simulation results for this new arrangement is shown in Fig. 4.7.

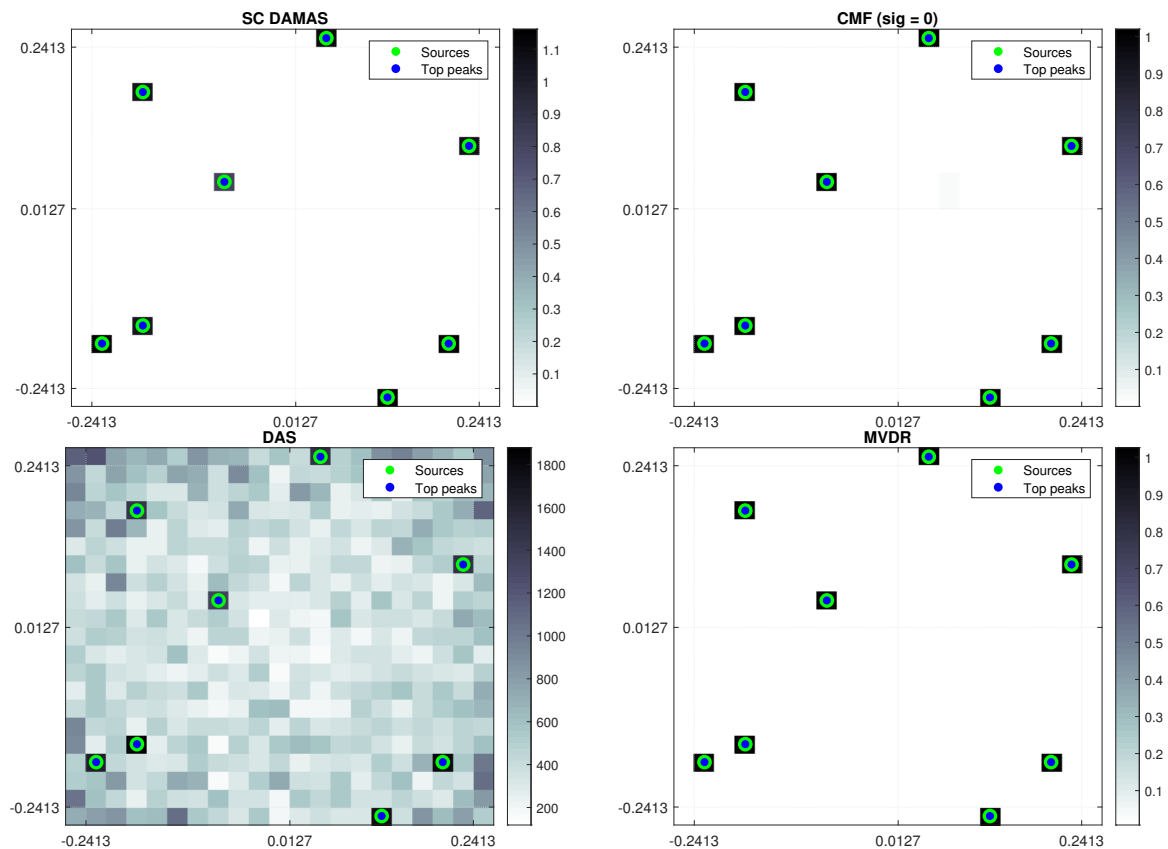


**Figure 4.7:** Acoustic Mapping with 33 sensors, frequency=15kHz and SNR: 20db

## 5 CONCLUSION

The source localization is performed using various algorithms that are successful in creating a map of source powers for the region of interest. We have seen the results from spectrum based beamforming approaches, deconvolution approach, along with delay and sum beamforming and direct optimization in the form of CMF. The effect of these algorithms with varying parameter such as noise levels and sensor number was studied.

The MVDR spectral search method performed increasingly well with a decrease in noise levels, or increase in sensor number, or increase in frequency. Furthermore, there seems to be some influence of the shape of sensor array on the region of source estimation for the Setup 1 2.1. In general, the MVDR method seems to perform best for cases where the sources are known to be well separated, else the side lobes in the MV spectrum can pose limitations to its capabilities. The Bartlett beamformer is an alternative to MVDR beamformer, but it has a lower resolution in most cases.

On the other hand, deconvolution techniques are introduced to improve the resolution limitations of the spectral search algorithms. We see that DAMAS and SC-DAMAS algorithms work on top of the delay-and-sum beamformer and deconvolve the spectrum to get an estimate of the original impulse response of the sources in the region of interest. We observe that the CMF method performs better than DAMAS and SC-DAMAS with an increase in noise levels. However when the sources were distanced farther from the sensors, SC-DAMAS seemed to perform better than the other two. In this case, the beamforming techniques like DAS and MVDR were the most robust.

This research can be further extended to incorporate a non-Free field medium in the acoustic mapping of the sources. In real world applications, it is rare to come across a free-field situation and therefore source localization algorithm for a non-free-field medium can be very productive. However, estimating the material properties of a medium that influence the acoustic response poses a whole different set of challenges.

## REFERENCES

- [1] Frank Neugebauer, Gabriel Möddel, Stefan Rampp, Martin Burger, and Carsten H Wolters. The effect of head model simplification on beamformer source localization. *Frontiers in neuroscience*, 11:625, 2017.
- [2] Zoujun Dai, Ying Peng, Hansen A Mansy, Richard H Sandler, and Thomas J Royston. Experimental and computational studies of sound transmission in a branching airway network embedded in a compliant viscoelastic medium. *Journal of sound and vibration*, 339:215–229, 2015.
- [3] Brian Henry and Thomas J Royston. A multiscale analytical model of bronchial airway acoustics. *The Journal of the Acoustical Society of America*, 142(4):1774–1783, 2017.
- [4] Brian Henry and Thomas J Royston. Localization of adventitious respiratory sounds. *The Journal of the Acoustical Society of America*, 143(3):1297–1307, 2018.
- [5] Keith Horsfield, Wendy Kemp, and Sally Phillips. An asymmetrical model of the airways of the dog lung. *Journal of Applied Physiology*, 52(1):21–26, 1982.
- [6] MB Ozer, S Acikgoz, TJ Royston, HA Mansy, and RH Sandler. Boundary element model for simulating sound propagation and source localization within the lungs. *The Journal of the Acoustical Society of America*, 122(1):657–671, 2007.
- [7] SM Akramus Salehin and Thushara D Abhayapala. Localizing lung sounds: Eigen basis decomposition for localizing sources within a circular array of sensors. *Journal of Signal Processing Systems*, 64(2):205–221, 2011.
- [8] Harry L Van Trees. *Optimum array processing: Part IV of detection, estimation, and modulation theory*. John Wiley & Sons, 2004.
- [9] Tarik Yardibi, Jian Li, Petre Stoica, and Louis N Cattafesta III. Sparsity constrained deconvolution approaches for acoustic source mapping. *The Journal of the Acoustical Society of America*, 123(5):2631–2642, 2008.
- [10] Thomas F Brooks and William M Humphreys. A deconvolution approach for the mapping of acoustic sources (damas) determined from phased microphone arrays. *Journal of Sound and Vibration*, 294(4-5):856–879, 2006.
- [11] Michael S Brandstein and Harvey F Silverman. A practical methodology for speech source localization with microphone arrays. *Computer Speech & Language*, 11(2):91–126, 1997.
- [12] Joseph H DiBiase, Harvey F Silverman, and Michael S Brandstein. Robust localization in reverberant rooms. In *Microphone Arrays*, pages 157–180. Springer, 2001.
- [13] Charles Knapp and Glifford Carter. The generalized correlation method for estimation of time delay. *IEEE transactions on acoustics, speech, and signal processing*, 24(4):320–327, 1976.
- [14] Ralph Schmidt. Multiple emitter location and signal parameter estimation. *IEEE*

*transactions on antennas and propagation*, 34(3):276–280, 1986.

- [15] Haley M Jones, Rodney A Kennedy, and Thushara D Abhayapala. On dimensionality of multipath fields: Spatial extent and richness. In *2002 IEEE International Conference on Acoustics, Speech, and Signal Processing*, volume 3, pages III–2837. IEEE, 2002.
- [16] Thomas Padois and Alain Berry. Two and three-dimensional sound source localization with beamforming and several deconvolution techniques. *Acta Acustica united with Acustica*, 103(3):392–400, 2017.
- [17] David L Donoho and Michael Elad. Optimally sparse representation in general (nonorthogonal) dictionaries via  $\ell_1\ell_1^1$  minimization. *Proc. Natl. Acad. Sci. USA*, 100(5):2197–2202, 2003.
- [18] Robert Tibshirani. Regression shrinkage and selection via the lasso. *Journal of the Royal Statistical Society: Series B (Methodological)*, 58(1):267–288, 1996.
- [19] Jos F Sturm. Using sedumi 1.02, a matlab toolbox for optimization over symmetric cones. *Optimization methods and software*, 11(1-4):625–653, 1999.